To be published in Journal of the Optical Society of America A:

Title: The refined EUV mask model

Authors: Igor Makhotkin,MEIYI WU,Victor Soltwisch,Frank Scholze,Vicky Philipsen

Accepted: 09 February 21

Posted 09 February 21

DOI: https://doi.org/10.1364/JOSAA.416235

© 2021 Optical Society of America

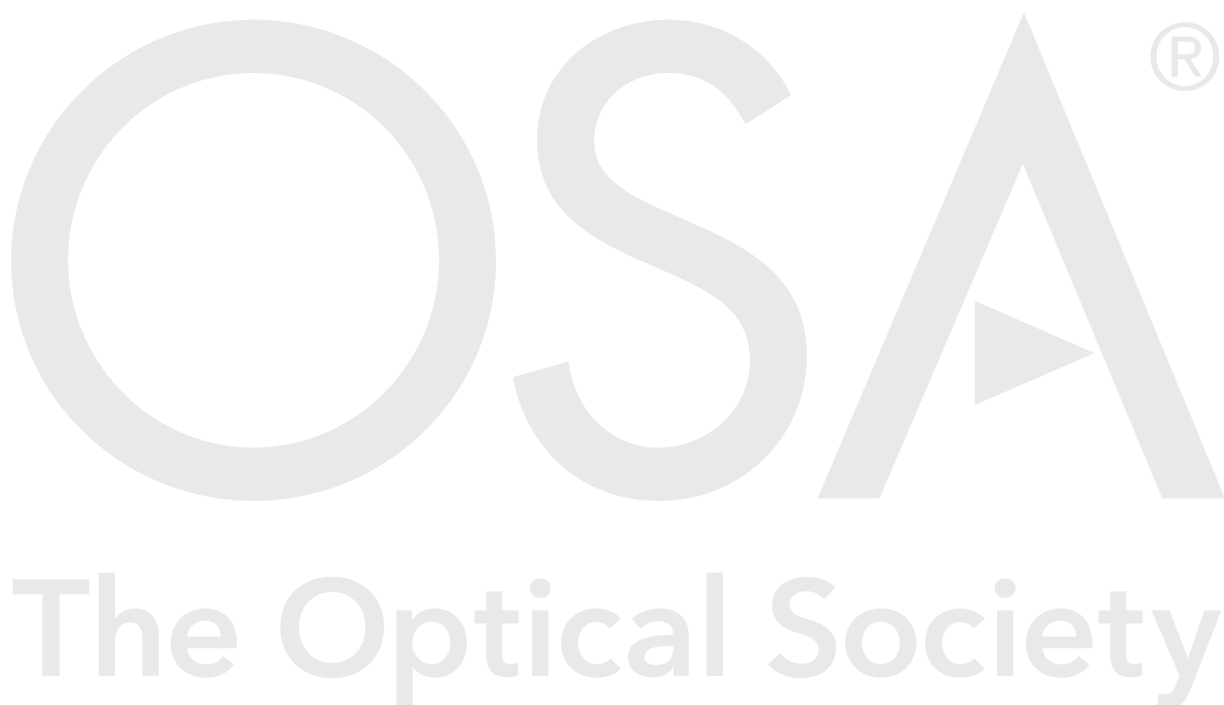

The refined EUV mask stack model

I.A. MAKHOTKIN[1]*, M. WU[1], V. SOLTWISCH[2], F. SCHOLZE[2], V. PHILIPSEN[1]

1.IMEC, Kapeldreef 75, 3001 Leuven, Belgium

2. Physikalisch-Technische Bundesanstalt, Abbestr. 2-12, 10587 Berlin, Germany

**i.makhtokin@utwente.nl*

Abstract: A refined model of an extreme ultraviolet (EUV) mask stack consisting of the Mo/Si multilayer coated by a Ru protective layer and a TaBN/TaBO absorber layer was developed to facilitate accurate simulations of EUV mask performance for high-NA EUV photo-lithography (EUVL) imaging. The model is derived by combined analysis of the measured EUV and X-ray reflectivity of an industry-representative mask blank. These two sets of measurements were analyzed using a combined free-form analysis procedure that delivers high-resolution X-ray and EUV optical constant depth profiles based on self-adapted sets of sublayers as thin as 0.25nm providing a more accurate description of the reflectivity than obtained from only EUV reflectivity. "Free-form analysis" means that the shape of the layer-interfaces in the model is determined experimentally and is not given a priori by the structure model. To reduce the numerical effort for EUV imaging simulations a low-resolution model of the multilayer and absorber stack with sublayer thicknesses larger than 2nm, that fits to only the EUV reflectance, was derived from the high-resolution model. Rigorous high-NA EUVL simulations were done to compare the performance of the new model to our previous work [1].

© 2020 Optical Society of America under the terms of the OSA Open Access Publishing Agreement

1. Introduction

The EUV mask is one of the key components of the photo lithography setup that can be designed and optimized by the end-user. The mask design largely determines the EUV lithography performance. The development of new masks is based on the large-scale numerical optimization of the EUV imaging quality by varying the parameters of the absorber patterns. Such mask optimization, as for example discussed in [2], can be used for the mitigation of mask 3D effects in order to improve EUV imaging.

A comprehensive understanding of the EUV mask stack (multilayer and absorber) is required to explore EUV imaging at high NA using rigorous mask 3D lithography simulations and to support EUVL at current NA 0.33 using full-field design modeling software. Current mask model was presented in 2013 [1] and is calibrated to the EUV reflectivity measured from the, at that time, industry-representative mask blank. The recent developments in mask making process as well as in EUV multilayer metrology calls for the model update. The detailed analysis of the structure of mask reflective multilayer is an essential input for the evaluation of the deposition optimizations as discussed for example here[3, 4].

The detailed study of the periodic multilayer EUV reflectivity (EUVR) analysis [5] showed that the single-wavelength EUV-only reflectivity measurement, although being very sensitive to minor structural changes of the multilayer, generally cannot be used for accurate determination of the sample structure because of the highly correlated influence of multilayer structural parameters, for example multilayer thickness ratio, densities and stoichiometries of layer materials. A minor change of the ratio between layer thicknesses in the multilayer model will change the simulated EUVR curve, however this change can be compensated by the change of total bi-layer thickness and layer density, making it impossible to determine accurate structural parameters from EUVR fit only [5].

To solve such correlation a combination of X-ray reflectivity (XRR) and EUVR measurements [5] was proposed, as well as the more complex combination of EUVR with scattering and X-ray fluorescence measurements [6]. In this paper, we will present a mask stack model – that simultaneously fits to both EUVR and XRR measurements of the actual mask. This combination allows us to accurately describe the structure and optical properties of the mask stack for EUV imaging. The implementation of the presented mask stack model in mask 3D aware simulation tools will enhance their predictive and pre-compensation power.

2. Mask measurements and data analysis

The presented model is built based on the analysis of two sample structures from current industry-representative EUV mask blanks. The first sample (referred to as MLM) is a periodic Mo/Si multilayer mirror containing 40 Mo-Si bilayers with the period thickness of 7nm deposited on SiO2 glass substrate. The multilayer is covered with a 3nm protective Ru layer. The second sample, referred to as absorber, is TaBN-TaBO absorber bi-layer with a thickness of 58nm and 2nm respectively deposited on the glass substrate coated with a 3nm thin Ru layer. In this set both samples have identical Ru layers and therefore the obtained models can be merged by overlapping the identical Ru layer.

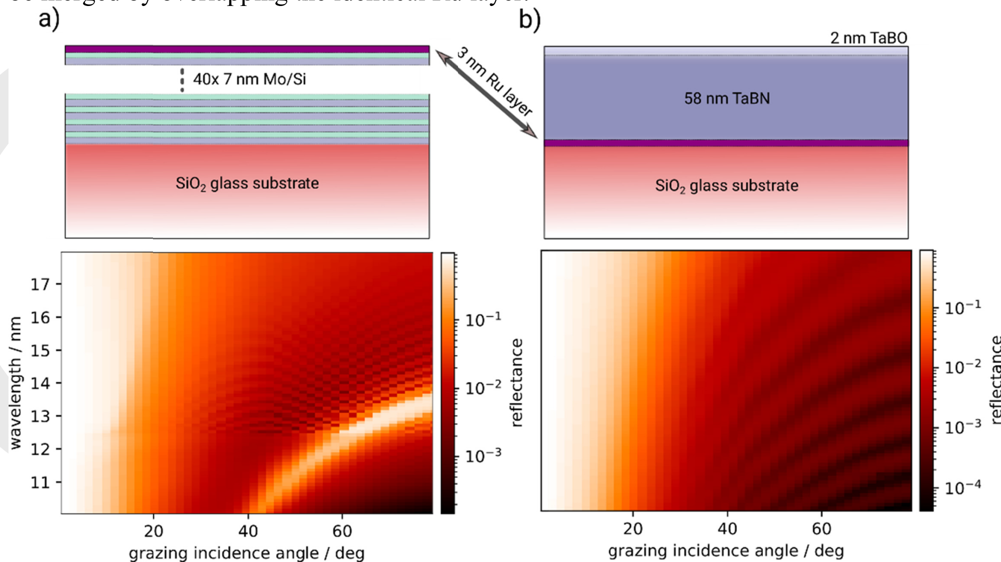

Fig. 1. Scheme of the a) Mo/Si multilayer and the b) TaBN/TaBO absorber layer with corresponding measured EUV reflectivity maps.

The Optical Society

The grazing incidence XRR is measured using Malvern Panalytical X'pert MRD XL multipurpose diffractometer equipped with a Cu X-ray source. For XRR measurements the Cu Kα_1 X-ray beam was conditioned, using the combination of parallel beam mirror and 4x Ge 220 monochromator enabling measurements of reflectivity of 0.154 nm over the large dynamic range of 10^7 counts per second with high resolution of 0.012 degrees, determined by the beam divergence. The XRR measurement angular range was limited by the measurement noise level of 0.1 counts per second. The EUV reflectivity measurements were conducted at the soft X-ray beamline of the Physikalisch-Technische Bundesanstalt at the electron storage ring BESSY II, which covers the photon energy range from 50 eV to 1900 eV. The beamline is equipped with a ultra-high vacuum lubrication free Ellipso-Scatterometer [7, 8]. The EUV reflectivity curves were measured using s-polarized radiation for the full accessible angular range from grazing incidence to near normal and mapped over the incidence wavelength from 10nm to 18nm. The experimental uncertainty is considered for every angle of incidence scan

separately to take into account for beam instabilities during the mapping. The schemes of the two measured samples together with EUV reflectivity maps are presented in Fig. 1. For the analysis of the sample structures, only the incidence angle scan at 13.5nm wavelength was used from the measured EUVR map. For the multilayer sample, the measurement angular range was limited to the most interesting for analysis region of normal incidence refection, for the absorber sample, the extended angular range from 0 to 80 degrees was measured. The data used for the analysis of XRR and EUVR are shown in Fig. 2a, 2b and 3a, 3b.

The analysis was performed by the following steps. The high-resolution profiles of the MLM and absorber samples are obtained using a modified free-form approach similar to that discussed by Zameshin et.al. in [9]. For a free-form analysis of X-ray and EUV reflectivity curves, the analyzed film is modelled as a set of thin sub-layers where the optical constants of each sublayer are determined by sub-layer chemical composition and density [5]. The stoichiometry values and densities were coded using the array of integers *P* as described in [10]. These values of *P* and total layer thickness were the only fitting parameter. In this way, a set of consistent optical constant profiles can be calculated for various wavelengths having equal sub-layer densities and stoichiometries and changing only wavelength-dependent atomic scattering factors [11]. The extended description of applied data analysis procedure is beyond the scope of the current paper and therefore will be published elsewhere.

The maximum thickness of the individual sublayer defines the in-depth resolution of the optically constant profile of the thin film and is determined by the measurement with the highest resolution. For both samples, the X-ray reflectivity determined the resolution of the high-resolution model to be 0.25nm corresponding to the measurement range of 9 degrees (Fig. 2a) at 0.154nm wavelength (see [9] for more details). For the XRR analysis of the absorber sample a sub-layer thickness of 0.5nm was used as the XRR measurement is informative only till 4 degrees (Fig. 3a). The profile steps in the Ru layer were kept as small as in the MLM model for the ease of the later merger of the models. Following the same logic, the minimal steps in both profiles to fit EUV reflectivity can be as large as 3.3nm assuming measurements at 13.5nm till 88 degrees grazing (2 degrees normal) incidence. Regardless of their low in-depth resolution, the EUVR data contribute to the combined analytical accuracy of the determination of densities and chemical stoichiometries of absorber and MLM models[5].

However, the fact that the optical constant model builds up from sublayers with a thickness of ~3.3nm can be accurate enough to fit the measured EUVR data, means that for EUV lithography simulations a low-resolution model can be build based on EUVR-only fitting, that produce as accurate as high-resolution model simulation results. Consequently, as a second step of the analysis, we obtain here the low-resolution models for MLM and absorber layer by fitting only the EUVR data. The initial guess model here was build based on the high-resolution model by combining its thin sublayers to thicker ones with averaged stoichiometries and densities.

OSA ® The Optical Society

2.1 The Mo/Si multilayer model

The measured and simulated (using best-fit results) X-ray and EUV reflectivity curves of the MLM sample are shown in Fig. 2a and 2b, respectively. The best fitted optical constants profiles, calculated for 13.5nm wavelength are shown in Fig. 2c by δ, the decrement of the real part of optical constant n, δ=real(1-n), while the fitted complex value of the optical constants n, β, can be found in Table 1.

In the δ-profile of the MLM sample (Fig. 2c) the Ru layer is shown between 0 and 7nm and the Mo/Si bilayer structure between 7nm and 14nm. We show the structure of only one Mo-Si bi-layer, because in our model we consider all 40 bi-layers to be identical. This assumption is supported by the good fit of the measured data, especially by the good agreement between the width of the measured and simulated Bragg peaks on the XRR curve.

The high-resolution profile shows the well-known interface asymmetry for the Mo/Si multilayer, namely the Mo-on-Si is larger than Si-on-Mo interface [12]. The characteristic ratio between the thickness of a reflector layer (here Mo) and total bi-layer thickness $\Gamma = 0.55$ is estimated for free-form profile shown on Fig. 2c as a ratio between the FWHM of Mo δ profile and a total thickness of the period. It should be noted that intrinsic multi-modality of both X-ray and EUV reflectivity analysis does not allow to claim determination of the exact profile shape. The extended research is on-going to understand and define precise error bars of free-form analysis.

The low-resolution profile of the periodic MLM part just roughly describes the high-resolution shape. However, as was mentioned afore, both high- and low-resolution profiles are equally good for the fitting of the EUVR measurements. Figure 2b shows that both new high- and low-resolution models fit much better to the new EUVR measurements than the previous model from 2013 [1], possibly due to the modification of the multilayer structure.

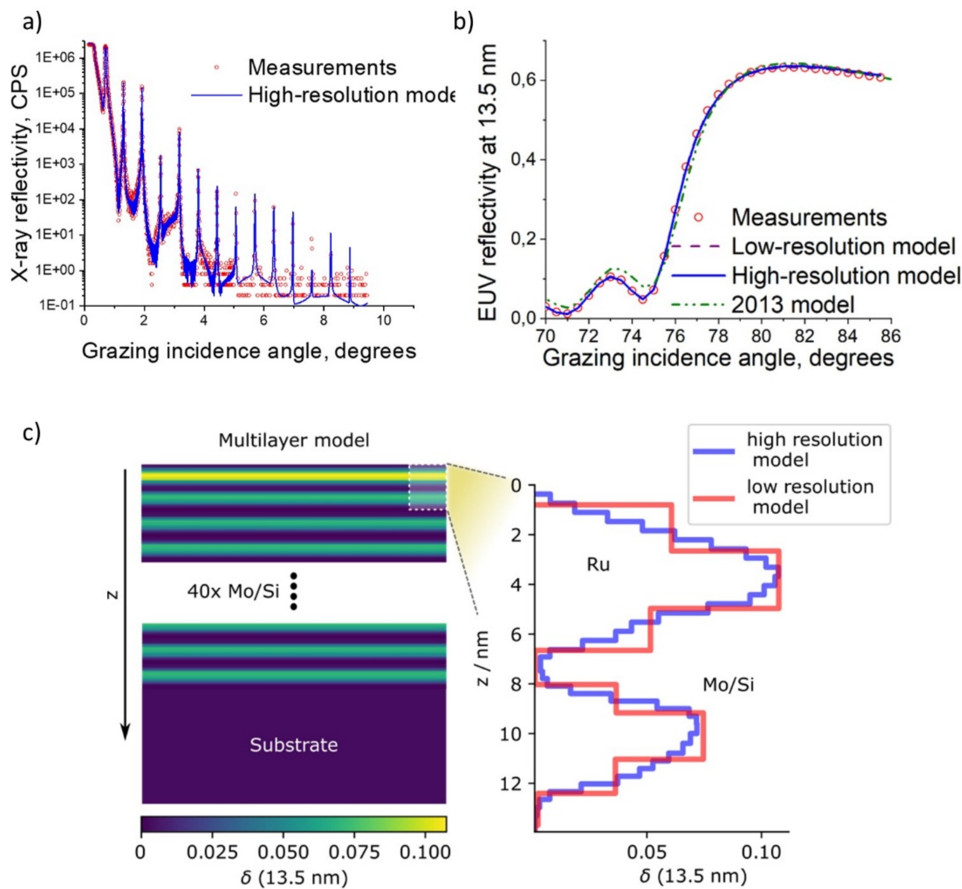

Fig. 2 (a) Measured XRR of the Mo/Si multilayer and its best fit solution. (b) Measured EUVR of the Mo/Si multilayer and the simulated EUVR from the low- and high-resolution multilayer model, as well as the simulated EUVR using the 2013 multilayer model. (c) The reconstructed low- and high-resolution δ-profiles for a single Mo/Si bi-layer calculated for EUV wavelength of 13.5nm.

2.2 The absorber model

The figures 3a and 3b show that the high-resolution model reasonably well fits to both X-ray and EUV reflectivity measurements. Figure 3b also shows that the low-resolution model fits as well to EUVR measurements than the high-resolution model. This is expected as the low-resolution model was obtained by fitting of EUVR-only measurements and presents one of

the deep local minima, while the high-resolution model can be seen as a Pareto optimal solution for the combined X-ray and EUV reflectivity data sets. The comparison between high- and low-resolution δ-profiles for 13.5nm wavelength and high-resolution profile for 0.154nm wavelength are shown in Fig. 3c.

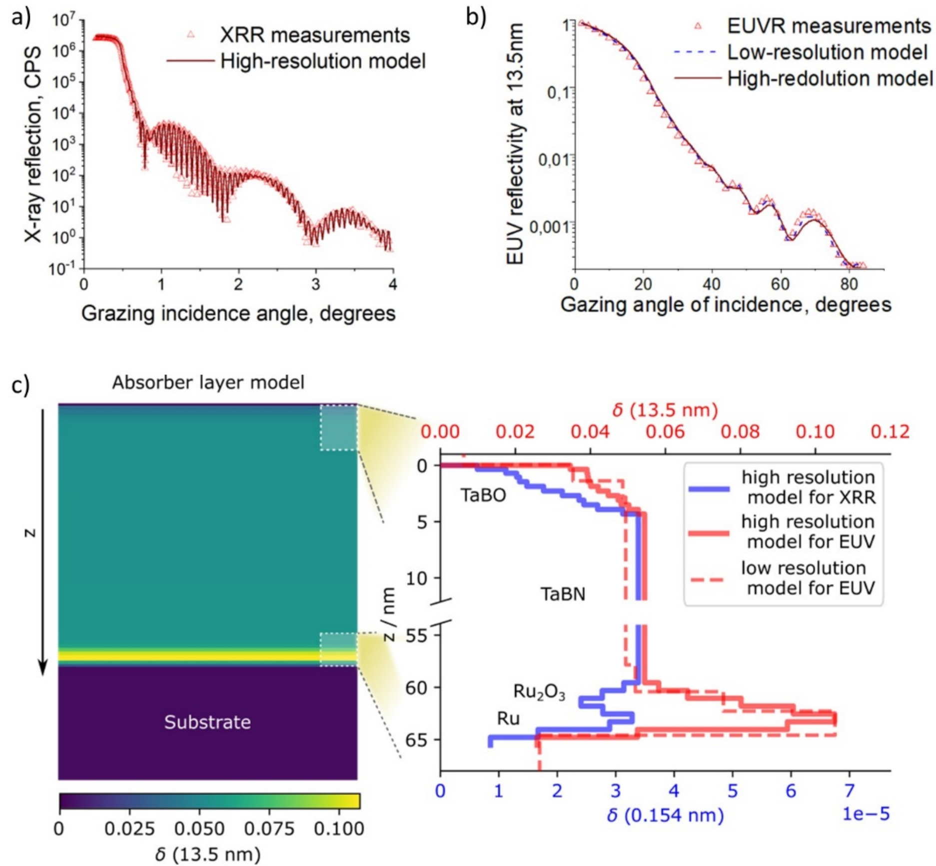

Fig. 3 Measured and best fit solutions for Ru/TaBN/TaBO thin film.(a) measured and best-fit high-resolution model calculated curves for XRR; (b) measured best-fit high- and low-resolution models for EUVR; (c) real part of decrement of the constants profiles (δ) shown for 0.154nm and 13.5nm wavelengths for high-resolution model together with low-resolution δ calculated only for 13.5nm wavelength.

The high-resolution absorber model was build based on initially known materials sequence: TaBO – TaBN – Ru- SiO_2 with few necessary modifications. First of all, we had to add ~1 nm of C-O layer as a first layer to account for C contamination. X-ray- only reflectivity would not be sensitive to this layer, as it can be interpreted as a part of top surface roughness. From the high-resolution model, we can conclude that only 55nm of the nominally 60nm thick absorber layer has a constant density while the rest is consumed by interfaces and transition layers. Fig. 3c shows that the top 2nm TaBO layer most likely forms only oxygen-rich interface transition regions.

We were not able to fit both X-ray and EUV reflectivity with smooth TaBN-Ru transition. The good fit required a remarkable drop, visible on the δ profile calculated for X-ray wavelength at z=60nm. As such profile drop, may be an indication of the presence of an oxidized Ru layer, what might be caused by exposure of the sample to ambient between

The Optical Society ®

depositions of Ru and Ta-based absorber layers, we have modelled it by introducing a possibility to add RuO_2 to this interface. At the same time, such deep is not visible on δ profile calculated for EUV because the 13.5nm light scatters much more effectively on oxygen atoms than X-rays due to proximity of O L absorption edge. Moreover, EUV radiation is almost entirely absorbed in the TaBN layer so EUVR is mostly sensitive to the top layer structure. It should be noted that as the uncertainty of EUV-only data analysis are quite large, the high- and low-resolution models can coincide within the uncertainty corridors of low-resolution profile.

For EUV lithography imaging simulations we have combined the low-resolution models of the multilayer and absorber layer stack. During the combination we fixed the Ru layer as it was determined for the MLM sample. The combined multilayer and absorber low-resolution model of the analyzed EUV mask is presented in Table 1. In the following part we compare the EUV lithography imaging simulations performed using the low-resolution model shown in Table 1 and presented in [1] in order to analyze the influence of the mask model on high-NA imaging.

Table 1. Low-resolution model for TaBO/TaBN absorber on a Ru/Mo/Si MLM mask.

Layer thickness,nm	Layer optical constants for 13.5nm EUV light ($1-\delta-\iota\beta$)
TaBO/TaBN absorber layer	
1.44	0.99375-0.00228i
1.44	0.96463-0.01841i
1.44	0.95139-0.03037i
55.02	0.95056-0.03163i
2.57	0.94800-0.03026i
Ru protective layer	
1.55	0.93925613-0.011132225i
2.465	0.89243499-0.016227441i
1.61	0.94843207-0.0088824872i
40x Mo/Si multilayer	
1.435	0.99889336-0.001918392i
1.215	0.96323059-0.0041547321i
1.807	0.92539394-0.0063108367i
1.422	0.96379023-0.0041027391i
1.151	0.9976784-0.0019250528i

3. Impact on key parameters in EUVL simulations

In the very recent paper[13] Mesilhy et al. studied in detail the effect of the reflectivity from various designs of multilayer masks in the lithography performance. To illustrate the effect of internal structure of the EUVL mask multilayer on the imaging we perform the imaging simulations for the anamorphic, high-NA EUV imaging. The EUV lithography simulations presented in this paper are performed with the rigorous mask 3D simulation software S-Litho EUV (Synopsys) [14]. Lines and spaces through pitch are imaged with a dipole leaf shape illumination at NA 0.55 using 4x/8x reduction system and 20% central obscuration of the projector pupil. The unpolarized EUV light is incident on the mask at 5.4 degree chief-ray angle[15]. The lines and spaces are evaluated over a pitch range from 16nm to 40nm, where the target critical dimension (CD) is the half-pitch value for pitches until 32nm and fixed to

The Optical Society ®

CD 16nm at larger pitches as can be seen on the curve target CD in Fig. 4a. The aerial image threshold is fixed to print the smallest pitch on target and the mask CD (MCD) required to print the other horizontal pitches to target at the fixed threshold is plotted in Fig. 4a. Lithography metrics such as best focus (BF), depth of focus (DoF), exposure latitude (EL) and telecentricity error (TE) are presented in Fig. 4.

The simulations denoted as "Low-res. model" are performed using the mask model presented in Table 1 and results denoted as "2013 model" are obtained with the mask model presented in [1].

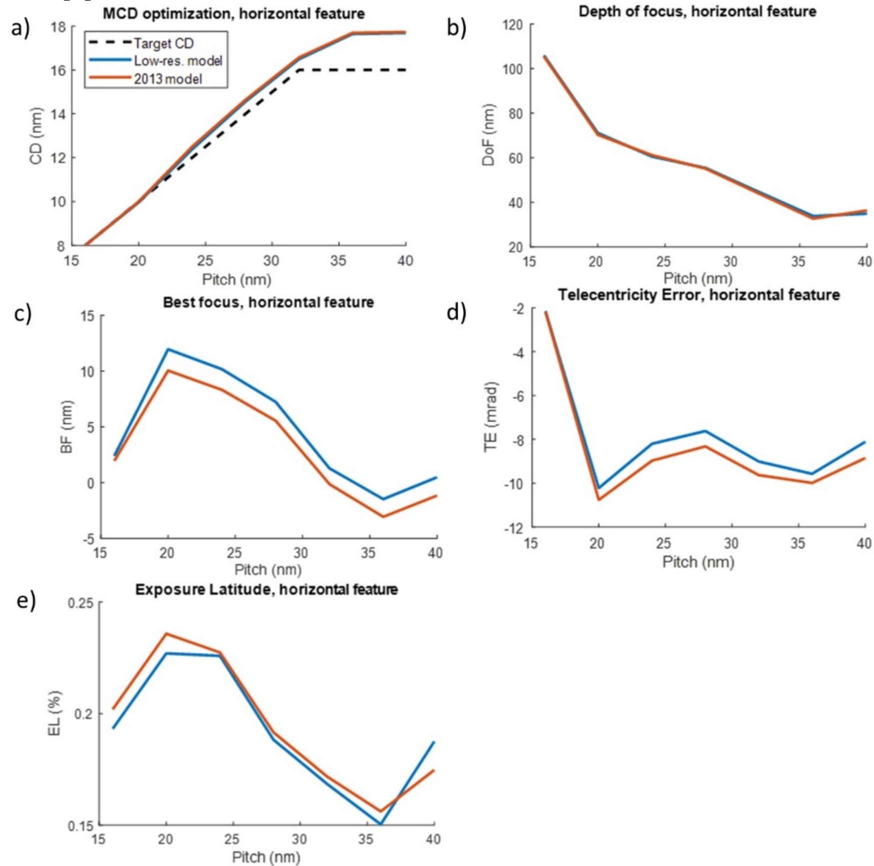

The Optical Society ®

Fig. 4 Comparison between EUVL metrics through pitch at high NA 0.55 calculated using the mask model presented here (denoted as Low-res. model) and presented in [1] (denoted as 2013 model).

Fig. 4 shows that regardless of the difference in the mask models there is not much difference between key EUVL metrics. The small differences can be explained by the relatively small influence of the EUVR for grazing incidence angles lower than 75 degrees (i.e., higher than 15 degrees from the normal) where EUVR curves differ most (see Fig. 2b).

4. Conclusions

We have analyzed the internal structure of the current industry-representative EUV mask blank using XRR and EUVR measurements. The high- and low-resolution models of the optical constant profiles from the mask blank are reported. The comparison of the mask model from 2013 to the newly proposed mask model is performed for next-generation high NA EUV simulation settings on lines and spaces. The simulations show that the slight

difference in measured EUVR at high incidence angles does not change the key EUVL metrics dramatically.

The high-resolution model gives an accurate description of the internal multilayer and absorber layer structures. The combined XRR and EUVR measurement of EUV mask blanks can be used to analyze changes in the multilayer and absorber structure in future mask R&D using the model described here as a reference.

Finally, we recommend the use of the new low-resolution mask model for next-generation EUVL simulations, as it fits better with the current industry-representative masks. The implementation of the presented low-resolution mask model should increase the simulation accuracy of more complex designs.

5. Funding, acknowledgments, and disclosures

6.1 Funding

This project has received funding from the Electronic Component Systems for European Leadership Joint Undertaking under grant agreement No 783247 - TAPES3. This Joint Undertaking receives support from the European Union’s Horizon 2020 research and innovation program alongside Netherlands, France, Belgium, Germany, Czech Republic, Austria, Hungary and Israel

6.2 Acknowledgments

We acknowledge dr. Sergey N. Yakunin for the assistance development of free-form analysis code of combined EUV-XRR data sets and dr. Joachim Woitok and Malvern Panalytical for the help with measurement of EUV mask blanks.

6.2 Disclosures

The authors declare no conflicts of interest.

References

1. V. Philipsen, E. Hendrickx, R. Jonckheere, N. Davydova, T. Fliervoet, and J. T. Neumann, *Actinic characterization and modeling of the EUV mask stack*, 29th European Mask and Lithography Conference (SPIE, 2013), Vol. 8886.
2. A. Erdmann, P. Evanschitzky, H. Mesilhy, V. Philipsen, E. Hendrickx, and M. Bauer, "Attenuated phase shift mask for extreme ultraviolet: can they mitigate three-dimensional mask effects?," Journal of Micro/Nanolithography, MEMS, and MOEMS **18**, 1-13, 13 (2018).
3. K. Rook, P. Turner, N. Srinivasan, T. Henry, K. Yamamoto, and M. Lee, *Process optimization for performance improvement in Mo/Si multilayers for EUV mask blanks*, SPIE Photomask Technology + EUV Lithography (SPIE, 2020), Vol. 11517.
4. N. Srinivasan, K. Rook, P. Turner, T. Henry, K. Yamamoto, D. Donnelly, T. V. Nguyen, V. Ip, M. Lee, S. Kohli, F. Cerio, and A. Devahasayam, *Interfacial quality of high-reflectivity Mo-Si multilayers for EUV mask blanks*, SPIE Photomask Technology + EUV Lithography (SPIE, 2019), Vol. 11147.
5. S. N. Yakunin, I. A. Makhotkin, K. V. Nikolaev, R. W. E. van de Kruijs, M. A. Chuev, and F. Bijkerk, "Combined EUV reflectance and X-ray reflectivity data analysis of periodic multilayer structures," Optics Express **22**, 20076-20086 (2014).
6. A. Haase, S. Bajt, P. Honicke, V. Soltwisch, and F. Scholze, "Multiparameter characterization of subnanometre Cr/Sc multilayers based on complementary measurements," Journal of Applied Crystallography **49**, 2161-2171 (2016).
7. C. Laubis, A. Barboutis, M. Biel, C. Buchholz, B. Dubrau, A. Fischer, A. Hesse, J. Puls, C. Stadelhoff, V. Soltwisch, and F. Scholze, "Status of EUV reflectometry at PTB," in *SPIE 8679, Extreme Ultraviolet (EUV) Lithography IV*, 2013), 867921-867921-867912.
8. F. Scholze, C. Laubis, K. V. Luong, and V. Philipsen, *Update on optical material properties for alternative EUV mask absorber materials*, 33rd European Mask and Lithography Conference (SPIE, 2017), Vol. 10446.

OSA® The Optical Society

9. A. Zameshin, I. A. Makhotkin, S. N. Yakunin, R. W. E. van de Kruijs, A. E. Yakshin, and F. Bijkerk, "Reconstruction of interfaces of periodic multilayers from X-ray reflectivity using a free-form approach," Journal of Applied Crystallography **49**, 1300-1307 (2016).
10. I. A. Makhotkin and S. N. Yakunin, "Model independent grazing incidence X-ray reflectivity " (2016).
11. B. L. Henke, E. M. Gullikson, and J. C. Davis, "X-Ray Interactions: Photoabsorption, Scattering, Transmission, and Reflection at E = 50-30,000 eV, Z = 1-92," Atomic Data and Nuclear Data Tables **54**, 181-342 (1993).
12. S. Braun, H. Mai, M. Moss, R. Scholz, and A. Leson, "Mo/Si Multilayers with Different Barrier Layers for Applications as Extreme Ultraviolet Mirrors," Japanese Journal of Applied Physics **41**, 4074-4081 (2002).
13. H. Mesilhy, P. Evanschitzky, G. Bottiglieri, E. van Setten, T. Fliervoet, and A. Erdmann, *Pathfinding the perfect EUV mask: the role of the multilayer*, SPIE Advanced Lithography (SPIE, 2020), Vol. 11323.
14. "http://www.synopsys.com/Tools/Manufacturing/MaskSynthesis/Pages/Sentaurus-Lithography.aspx" (2019), retrieved.
15. E. v. Setten, G. Bottiglieri, L. d. Winter, J. McNamara, P. Rusu, J. Lubkoll, G. Rispens, J. v. Schoot, J. T. Neumann, M. Roesch, and B. Kneer, *Edge placement error control and Mask3D effects in High-NA anamorphic EUV lithography*, SPIE Photomask Technology and EUV Lithography (SPIE, 2017), Vol. 10450.